

Diffusion of Tungsten in Chromium: Experiments and Atomistic Modeling

Mansoo Park, Kathleen C. Alexander, and Christopher A. Schuh*

*Department of Materials Science and Engineering, Massachusetts Institute of Technology
77 Massachusetts Ave, Cambridge, MA 02139, USA*

*Corresponding Author: email: schuh@mit.edu Tel: +44 617-253-6901

Abstract

The solute diffusion of tungsten at low concentrations in chromium has been investigated both by experiments and computational methods. From finite-source diffusion experiments measured with an Electron Probe Micro Analyzer at temperatures from 1526–1676 K, it was found that the diffusivity of tungsten in chromium follows the Arrhenius relationship $D = D_0 \exp(-Q/RT)$, where the activation energy was found to be $Q = 386 \pm 33$ kJ/mol. Diffusion of tungsten in chromium was investigated computationally with both the activation-relaxation technique (ART) and molecular dynamics (MD) using a hybrid potential. From ART, the effective diffusion activation energy was determined to be $Q = 315 \pm 20$ kJ/mol based on a multi-frequency model for a monovacancy mechanism. From MD, the square displacement of tungsten was analyzed at temperatures between 1200 and 1700 K, and the diffusion activation energy was determined to be $Q = 310 \pm 18$ kJ/mol. In spite of possible complications arising due to experimental compositions away from the dilute limit, the agreement between experiments and simulations falls within the calculated uncertainties, supporting a monovacancy mechanism for diffusion of tungsten in chromium.

Keywords: High-temperature alloys, Diffusion, Clusters, Vacancy formation, Chromium, Tungsten

1. Introduction

Because it is often used at elevated temperatures, diffusion in chromium (Cr) has been studied experimentally, theoretically, and computationally for decades [1–15]. Although there were some early discrepancies regarding the mechanisms and activation energy of Cr self-diffusion [1,10–12], these were eventually resolved and Cr self-diffusion is now believed to follow the normal mechanisms identified for other BCC metals [1,10], namely, monovacancy diffusion at lower temperatures, with a contribution from divacancy diffusion at higher temperatures (generally above about 1700 to 2000 K [4,14]). Additionally, there exists a large body of work regarding diffusion in a number of Cr-alloys [9,16–22]. Diffusion in chromium-tungsten (Cr-W) alloys is among the least studied of these binary systems, with Ref. [23] providing the only discussion of it of which we are aware, and that being a qualitative analysis of Cr-W grain boundary diffusion.

As tungsten (W) is only mildly soluble in Cr, it is not surprising that this couple has not previously been given much attention. However, recent work on the stability of nanocrystalline alloys [24,25] indicates that Cr-W is a good candidate system to form stable nanocrystalline phases [24]. The possibility of fabricating nanocrystalline alloys with superior strength, hardness, and thermal stability in the Cr-W system is compelling, and our group's unpublished work on the processing of such alloys also led us to appreciate the need for a better understanding of the kinetics of the system. It is therefore our purpose in the present paper to address the gap in kinetic data in the literature for the diffusion of W in Cr.

In this study, Cr-W diffusion was investigated experimentally at temperatures in the range 1526–1676

K in the low-concentration solid solution regime (i.e., W content below the solubility limit of ~30%) that is most relevant to applications of the Cr-W system. To complement this experimental work and more explicitly connect to the dilute limit, computational studies of dilute C-W systems were also performed. The activation-relaxation technique (ART) [26,27] was used to investigate the energies of the accessible atomic structure transitions at a vacancy in a Cr-W system. Additionally, the diffusion of a single W atom in Cr was investigated with molecular dynamics simulations at temperatures between 1200 and 1700 K.

2. Experiments

Chromium discs (99.9% purity, 10 mm diameter, 5 mm thickness, from Alfa Aesar) were ground flat and parallel. To induce grain growth, the specimens were annealed at 1675 K for 24 hours. The final grain size was about 350–400 μm . A thin film (~1 μm) of high-purity tungsten (99.95%, from Alfa Aesar) was deposited on each disc by physical vapor deposition for 3 hours using an in-house sputter system operated under 155 W of RF power (from CESAR), while flowing 10 sccm Ar gas, with the chamber vacuum maintained below 10^{-7} Torr.

Each specimen was sealed in a quartz tube, first evacuated to 10^{-6} Torr using a turbo pump, and then backfilled with high-purity argon gas to 120 Torr. The sealed specimen was annealed in a furnace and exposed to temperatures of 1526, 1550, 1576, 1627, and 1676 K for 398, 212, 120, 48, and 22 hours, respectively. The diffusion depth in all cases was around 40 μm . After annealing, each specimen was laid on its side, embedded in an electrically conductive resin, and ground through half of its full width using an automatic polisher (TegraForce-5 from Struers) to expose the diffusion cross-section. A right angle between the side and top surface was achieved to within 0.2 degrees. An Electron Probe Micro Analyzer (EPMA, JXA-8200 from JEOL) was then used to obtain depth profiles of tungsten concentration in chromium. For each specimen, 5–12 concentration profiles were acquired, spaced at least 20 μm apart.

A cross section of a chromium disc after tungsten diffusion is shown in Figure 1, where the image contrast from backscattered electrons and the inset energy-dispersive spectroscopy (EDS) map show the local tungsten content. The tungsten diffusion profile is uniform along the long axes of the specimen and approximates one-dimensional diffusion well.

Tungsten concentration as a function of diffusion depth at five different temperatures measured using EPMA is shown in Figure 2. The diffusion of W into Cr in this experimental setup follows that for a semi-infinite one-dimensional solution of Fick's second law with a limited diffusant source:

$$C(x, t) = \frac{M}{\sqrt{\pi Dt}} \exp\left(-\frac{x^2}{4Dt}\right) \quad (1)$$

Here, C is the concentration of tungsten at a distance x from the initial Cr-W interface after diffusion time t , and M is the total amount of deposited tungsten. D is the solute self-diffusion coefficient of tungsten in chromium. Concentration was converted to specific activity and is plotted vs. x^2 in Figure 3. Specific activity was obtained from concentration through division by the specimen density in any convenient units; for the data in Figure 3, the units of density were chosen for each profile so as to provide uniform separation of the curves. From a fit of Eq. (1) to the data in Figure 3 (with M treated as an unknown fitting parameter at each temperature), the diffusion coefficient was determined for each specimen (correlation coefficients $R^2 > 0.98$ were obtained for each profile), as listed in Table 1, and an

Arrhenius plot of $\ln D$ vs. $1/T$ is presented in Figure 4. In Eq. (1), D is assumed to be independent of concentration; the use of this equation is valid in the present study because $\log(\text{activity})$ vs x^2 was found to be linear and the thickness of the deposited solute layer was less than $1\mu\text{m}$, which is much less than $(Dt)^{1/2}$ for every investigated temperature.

The equation for the solute diffusion of tungsten in chromium can be described by an Arrhenius relationship:

$$D = D_0 \exp\left(-\frac{Q}{RT}\right) \quad (2)$$

A least squares regression analysis of the data from Figure 4 yields the activation energy, $Q = 386 \pm 33$ kJ/mol and the diffusion prefactor, $D_0 = A_0 \exp(-6.8 \pm 2.5)$ m²/s where A_0 is the unit measure of diffusivity: 1 m²/s, and the reported uncertainty ranges correspond to 95% confidence bounds.

3. Computations

3.1 Cr-W Potential and Vacancy Structure

The initial configuration, generated with the open-source Large-scale Atomic/Molecular Massively Parallel Simulator (LAMMPS) software package [28,29], was a pure, single crystal of BCC Cr with periodic boundary conditions in all directions and initial geometry minimized according to the concentration-dependent embedded atom method (CD-EAM) potential developed by Stukowski et al. [30–32]. This potential was developed to study BCC Fe-Cr alloys throughout the full compositional range and was verified to satisfactorily reproduce the self-diffusion behavior of pure chromium with a monovacancy migration energy of 0.99 eV [6].

One atom was removed from the single-crystal structure of pure Cr to generate a vacancy, and the system geometry was minimized again with the Stukowski CD-EAM potential. The vacancy formation energy in Cr was determined to be 2.56 eV, in agreement with previously reported results [16]; this value is calculated by taking the difference between the total energy of the system containing a vacancy and a perfect crystal with the same number of atoms. One Cr atom adjacent to the vacancy was then replaced with a W atom, and a hybrid potential was used to minimize the system. In the hybrid potential, the Cr-Cr interactions were again modelled with the Stukowski CD-EAM potential, and the W-Cr interactions were modelled with the cubic-spline pair potential developed by Bonny et al. [18]. As the system being investigated was low in concentration, only one W atom was present in the computational setup, and no W-W interactions were considered. The results presented herein correspond to a system of 431 total atoms in a cubic supercell with 1.7 nm length edges. For verification of the results, a system with 3455 total atoms was also considered, corresponding to a cubic supercell with 3.45 nm edge length, yielding results that did not differ significantly from the smaller system.

A binding energy between W and the vacancy was observed. When the vacancy was separated from the W, the system was found to be 0.66 eV higher in energy than when W was bound to the vacancy. Images of the configurations of the vacancy structure when bound to a W atom and sufficiently removed from the W atom are shown in Figure 5. Atoms that were not in the vacancy structure were excluded from this figure. Atoms are colored according to centrosymmetry [33] with the scale shown.

From Figure 5, it is apparent that the W atom introduces an asymmetry into the vacancy structure that

is not present in the unbound vacancy. Intermediate structures with intermediate energies (0.54 and 0.59 eV above the minimum energy structure) were found for the cases where W was a nearest neighbor and next-nearest neighbor to the vacancy. A schematic showing all relevant locations of the W atom with respect to the vacancy is shown in Figure 6, and their relative energy levels are presented in Table 2.

3.2 Local Transitions at a Vacancy

3.2.1 The Activation-Relaxation Technique

The activation-relaxation technique (ART) was implemented to determine the kinetic transitions accessible to the Cr-W alloy system at a vacancy. ART is an algorithm for finding transition states in a potential energy landscape when only the initial configuration is known [26,27] and consists of each a perturbation, convergence, and relaxation phase. In the perturbation phase, the Cr-W atomic configuration in a minimum energy state was locally perturbed until the lowest eigenvalue of the Hessian matrix, λ_{\min} , was less than a small negative number, $\lambda_c = -1.0$. The perturbation event consisted of choosing a random atom in the vicinity of the defect and displacing it in a random direction by a random distance in the range 0.5 – 2.0 Å. An atom was deemed to be in the vicinity of the defect if its centrosymmetry parameter [33] was larger than a critical value of 0.1.

In the convergence phase of ART, the system was iteratively pushed along the eigenvector corresponding to the lowest eigenvalue of the Hessian matrix and relaxed in the hyperplane of this vector until either a transition state was converged upon or an alternative exit condition was met. A transition state had to meet the requirements: $\lambda_{\min} < 0$ and $f_{\max} < f_{\text{tol}}$, where f_{\max} refers to the maximum force in any direction on any atom, and here, $f_{\text{tol}} = 0.005$ eV/Å was used. Alternative exit conditions for the convergence phase of the algorithm included reaching either a configuration with $\lambda_{\min} > 0$ or the maximum number of convergence steps, prescribed here as 100. If a transition state was found in the convergence phase, its connectivity to the initial minimum was then checked [34], and if it was determined that the transition state was connected to the initial minimum, the algorithm proceeded to the relaxation phase. If any of the requirements for a transition state were not met or the transition state was not found to be connected to the initial minimum, the search was deemed unsuccessful.

The relaxation phase of the algorithm consisted of a constant-stress conjugate gradient relaxation (with all elements of the stress tensor set to zero) from the transition state to an adjacent minimum, which was achieved by pushing the atomic configuration at the transition state slightly away from the initial minimum configuration prior to the minimization. This relaxation was performed in LAMMPS using the same hybrid potential as discussed in Section 3.1.

This ART procedure was repeated many times with different random perturbations in order for the space of possible transitions accessible to the system to be sufficiently explored. The search was deemed complete when no new transitions were identified for 100 consecutive successful searches.

In all cases, the forces throughout the system were determined in LAMMPS using the hybrid potential described in Section 3.1. The minimum eigenvalue was approximated using the Lanczos method [35,36] with a maximum number of iterations: $L_N = 15$. If L_N Lanczos iterations were completed before other exit conditions of the algorithm were reached, convergence was tested by comparing the residual to a cutoff value, here: 0.1. If the convergence test failed, then the Lanczos method was implicitly restarted, where the most recently calculated eigenvector was used as the initial guess to

initialize the method [36]. It should be noted that, in this discussion, the term ‘residual’ is a measure of the quality of the approximated eigenvalue-eigenvector pair and is calculated as: $|Av - \lambda v|$ for matrix A , approximate eigenvector v , and eigenvalue λ . This implicit restarting procedure was repeated until either the residual was lower than the specified value or Lanczos method had been attempted L_N times.

Within the Lanczos method, it is possible to obviate the need for explicitly calculating the Hessian matrix by instead approximating the product of the Hessian matrix, $H(x_n)$, with the j th vector of the Krylov subspace, v_j , using a second order finite difference approximation:

$$H(x_n)v_j \approx \frac{1}{2\epsilon} \left(\nabla f(x_n + \epsilon v_j) - \nabla f(x_n - \epsilon v_j) \right) \quad (3)$$

Where f is the potential energy function and, consequently, $-\nabla f$ is the $3N$ force vector for the system (N being the number of atoms in the system). This approach allowed for significant improvements in computational efficiency compared with the direct method.

The energy landscape data found with ART was post-processed by first synthesizing the data such that only unique transitions were included in further analysis. Two transitions were considered non-unique if their respective transition state and adjacent minimum energies were identical to the nearest 0.01 eV and the centrosymmetries of their respective atoms in the defect region were sufficiently similar (within 0.1). Additionally, transitions for which the adjacent minimum energy, E_{adj} , was within kT of the transition state energy, E_a , were excluded from further analysis as the reverse reaction rate for these structures to fall back down to the initial minimum would be very large compared to the forward reaction rate. $T = 1673$ K was used for this criterion, so transitions for which the difference $E_a - E_{adj} < kT = 0.14$ eV were neglected.

3.2.2 Local Transitions from ART

A schematic relevant to solute diffusion in dilute alloys is presented in Figure 6 and will be useful in discussing the results of ART. The post-processed data from ART is summarized in Table 2 including the type of transition corresponding to Figure 6, the activation energy of the transition, and the final energy of the configuration after the transition, both relative to the lowest energy structure. Although multiple mechanisms were found for some transitions, all activation energies reported in Table 2 correspond to the lowest energy mechanism found. It should be noted that only the jump corresponding to ω_{1W} results in any motion of the tungsten atom. However, the relative jump frequencies of all the events accessible to the bound vacancy must be considered in correctly analyzing the solute diffusion of W in Cr. In particular, these other frequencies are important in determining the correlation coefficient and vacancy escape frequency [15,37] as discussed in Section 3.2.3. The activation energies for the reverse jumps can be calculated from Table 2 as the difference: $E_{rev} = E_a - E_{adj}$.

The transition in which the vacancy moves to position 4 in Figure 6 corresponds to the separation of the vacancy from the tungsten, such that the final structure is 0.66 eV higher in energy than that of the bound structure. Additionally, when the vacancy moves to position 2 in Figure 6, the total energy of the structure is actually higher in energy than the unbound state by 0.07 eV, resulting in a repulsive interaction between the W and the vacancy.

A visual summary of all the transitions found with ART for this system, once again including only the lowest energy mechanisms, is presented in Figure 7, plotted as an energy landscape graph [38].

Important features of these transitions including the energy at the transition state, E_a , and the energy of the adjacent minimum configuration, E_{adj} (both shown in eV relative to the initial minimum), can be read directly from Figure 7. For clarity, the transitions have each been labeled to correspond to the jump frequencies in Figure 6.

3.2.3 Determination of Diffusivity from ART Transitions

Solute diffusivity, D_S , can be calculated from the jump frequencies in Figures 6 and 7 according to:

$$D_S = a^2 f_S \omega_S \exp[-(G_v^f + G_v^b)/kT] \quad (4)$$

Where a is the lattice parameter, ω_S is the jump frequency for the solute to exchange with the vacancy (ω_{1W} in our model), G_v^f is the formation energy of a vacancy in pure Cr (2.56 eV), and G_v^b is the binding energy of the solute atom with the vacancy, which is negative when attractive, (-0.66 eV for W in Cr). The correlation factor, f_S , depends on the other jump frequency terms in Figure 6 according to an equation developed by Manning [37] for dilute BCC systems:

$$f_S = \frac{7F\omega_{\beta m}}{2\omega_S + 7F\omega_{\beta m}} \quad (5)$$

$\omega_{\beta m}$ is defined as the jump frequency for the vacancy to move between the first- and third- or fifth-nearest neighbor site with respect to the solute atom, and $7F$ is defined by Manning [37] as:

$$7F = \frac{331.14 \left(\frac{\omega_{j\beta}}{\omega_{jm}}\right)^2 + 857.93 \left(\frac{\omega_{j\beta}}{\omega_{jm}}\right) + 409.95}{165.57 \left(\frac{\omega_{j\beta}}{\omega_{jm}}\right) + 134.21} \quad (6)$$

With $\omega_{j\beta}$ being the jump frequency for the vacancy to move from a second- to a first- nearest neighbor position and ω_{jm} being the jump frequency for the vacancy to move from a second- to a fourth- nearest neighbor position with respect to the W atom.

In the present analysis, instead of using the traditional geometrical definition of nearest neighbor based on the shortest Cartesian distance, we choose the site with the lowest activation barrier as the ‘nearest neighbor’ in order to accurately determine the escape frequency. Similarly, the second- and third-nearest neighbors are those with increasingly higher activation barriers. We note that the geometry and symmetry arguments used to develop Eqs. (5-6) assumed both that the traditional nearest neighbor definition was used and that the binding of the second-nearest neighbor was much stronger than for the third- or fifth-nearest neighbors. The approach used here conforms to the latter assumption, and usually also yields neighbor orderings consistent with the geometrical approach as well.

Thus, in the calculations performed here: $\omega_{j\beta} = \omega_{51}$, $\omega_{jm} = \omega_{54}$ (where $E_{a,jm} = E_{a,54} = 0.89$ eV was found with ART), and $\omega_{\beta m} = \omega_{12}$. In all cases, jump frequency was related to the activation energy of the transition by:

$$\omega_{ij} = \nu_{ij}^* \exp(-E_{a,ij}/kT) \quad (7)$$

Where ν_{ij}^* is the effective frequency for a transition from position i to position j . This value is defined by Vineyard [39] as the ratio of the products of all real vibrational frequencies in the initial state to all the real vibrational frequencies in the transition state:

$$\nu^* = \left(\prod_{i=1}^N \nu_i \right) / \left(\prod_{i=1}^{N-1} \nu'_i \right) \quad (8)$$

Under the harmonic approximation, the vibrational modes themselves can be calculated from the eigenvalues of the mass-normalized Hessian matrix (i.e. $H_{ij}^m = H_{ij} / \sqrt{m_i m_j}$). Thus, for each transition of interest, the mass-normalized Hessian matrix was calculated using a centered difference approximation with the potential described in Section 3.1. The eigenvalues, λ_i , of the normalized Hessian matrix for both the initial configuration and saddle point were then determined using standard LAPACK routines [40]. From the eigenvalues, the vibrational modes were calculated according to:

$$\nu_i = \frac{1}{2\pi} \sqrt{\lambda_i} \quad (9)$$

All real vibrational modes were then used in Eq. (8) to determine the effective transition frequency, ν^* . The effective transition frequency for each of the transitions required in order to calculate D_S are shown in Table 3.

Using the values in Tables 2 and 3, D_S was calculated according to Eq. (4) at temperatures between 1200 and 1700 K. An Arrhenius fit of the data is presented in Figure 8.

From a linear fit of the data in Figure 8, we find that the effective activation energy for W diffusion in Cr given a monovacancy mechanism is $Q = 315 \pm 20$ kJ/mol, and the pre-exponential term is $D_0 = A_0 \exp(-11 \pm 2.5) \text{ m}^2/\text{s}$, where A_0 is again the unit measure of diffusivity: $1 \text{ m}^2/\text{s}$. Uncertainty associated with these values derives both from the inherent uncertainties in the potentials used to model the system as well as from the assumptions that lead to the calculation of the correlation factor including consideration of only mechanisms within a traditional ‘single-jump’ distance and the use of the harmonic approximation. We estimate these uncertainties as amounting to perhaps ± 20 kJ/mol in the activation energy and ± 2.5 in the constant of the linearized Arrhenius model based on the range of values these terms can take when the input activation energies in Eq. (4) are varied (individually) by 0.2 eV— a reasonable assumption of the error associated with the potential.

3.3 MD of Many Transitions

3.3.1 Molecular Dynamics Procedure

The system, generated as described in Section 3.1, was annealed at temperatures in the range 1200–1700 K. The system was brought to the target temperature by a staged equilibration process in increments of 300 K for 300 picoseconds each, with a timestep of 1 femtosecond, temperature and pressure held constant, and an additional Berendsen barostat used to moderate the pressure [41]. After equilibrating in this manner at the target temperature, the simulation was run for 100 nanoseconds, with a timestep of 1 femtosecond, at constant temperature and volume, again with a Berendsen barostat. At each stage, the target pressure in the system was set to zero.

During the final stage of the MD simulation, the displacement of all atoms was tracked at every 10,000 steps. When this data was post-processed, resampling was achieved by treating each step in the simulation as its own initial configuration so that a mean square displacement for each possible time interval could be calculated. Diffusivity was then calculated based on the relation: $\langle(x - x_0)^2\rangle = 6Dt$, which assumes an isotropic diffusion model. The slope of the mean squared displacement curve vs. time was then taken as an estimate of the diffusivity of W in Cr at each temperature investigated.

It should be noted that the slope of the mean squared displacement least-squares fit had to be rescaled to account for a discrepancy between the expected vacancy fraction in a physical specimen of Cr at the temperature of interest and the vacancy fraction in the system generated for this simulation. Namely, the correction: $D' = f_{actual}/f_{simulation} D$, was used, where the vacancy fraction follows the Arrhenius form: $f = \exp(-G_v^f/kT)$.

3.3.2 Molecular Dynamics Results and Discussion

The activation energy for diffusion of W in Cr was estimated from the MD data (based on an enforced monovacancy mechanism) in the same fashion as the experimental data analysis presented in Section 2. The Arrhenius representation of the diffusivities determined at 11 different temperatures between 1200 and 1700 K is presented in Figure 9. From this treatment, it was calculated that $Q = 310 \pm 18$ kJ/mol with 95% confidence bounds and $D_0 = A_0 \exp(13.7 \pm 1.5) \text{ m}^2/\text{s}$, with A_0 the unit measure of diffusivity: $1 \text{ m}^2/\text{s}$.

4. Discussion

A summary of the results for the activation energy and diffusion prefactor for diffusion of W in Cr as determined by all three methods is presented in Table 4. The activation energies determined with the computational results are in excellent agreement with one another. To some extent, this can be regarded as a validation of the methodology used in connection with Eqs. (5-6) and the use of an energy-based ordering of atomic neighbors, since the MD results do not depend on that analysis and return the same essential output with regard to the diffusion activation energy. However, the diffusion values predicted by these two approaches differ by about an order of magnitude due to the discrepancy in their diffusion prefactor estimates. This difference may be related to the harmonic approximation assumed in the multiple frequency analysis; i.e., anharmonic effects may be relevant in the present temperature range. However, since validation with a system containing 3455 atoms did not show significantly different diffusion behavior from the 431 atom system, we do not expect this to be a major factor at these temperatures. Alternatively, it may be an indication that the empirical values in Eqs. (5-6) are not optimized for diffusion in the Cr-W system.

While there is a non-negligible difference between the computational and experimental activation energies of order 20%, this is an apparent inconsistency on the slope of the data and not of the diffusivity values themselves. This can be seen in Figure 10, where diffusivity data for all three methods has been overlaid, and the agreement is good within uncertainty. The experimental data lie between those of the models, and actually lie within the error bands of both of the two methods, which is encouraging.

A number of features of the computational approach may have contributed to the observed mild disagreement between the activation energies determined by the experimental results and models. These include the use of a highly-simplified model in which only monovacancy mechanisms were

considered and W-W interactions were ignored. Additionally, the accuracy of both computational methods was highly dependent on the quality of the potential used to model the system, which is uncertain. Alternatively, whereas in a very dilute alloy the assumed simple monovacancy mechanism may be of the only contributing mechanism to diffusion in this system; however, the experimental system in this study involved concentrations up to about 7 atomic % W, where W-W interactions may play a role.

To investigate this last possibility, a computational system with multiple tungsten atoms was considered. In particular, a system was built as in Section 3.1, and then a Cr atom in the vacancy structure was replaced with a W atom, such that the final system contained two W atoms in the vacancy structure. The system was minimized using the hybrid potential described in Section 3.1 with the addition of another EAM potential to account for W-W interactions [42]. ART was then performed on this system in order to find the transitions accessible to a vacancy with two adjacent W atoms as well as the binding energy of the vacancy to the tungsten pair. Additionally, the importance of W-W clusters was considered by comparing the relative energy of a system with adjacent W atoms to a system with two separated W atoms.

From these simulations, it was found that separation of the two W atoms resulted in an energy penalty of 5.05 eV, which indicates a strong likelihood that the W atoms would be found in pairs or possibly clusters of higher order in a non-dilute alloy. Additionally, it was found that the binding energy of a vacancy to the W atom pair was -0.54 eV, which is 0.12 eV less attractive than the interaction between a single W atom and a vacancy. From these features, one could conjecture that the diffusivity of W in this system may involve a contribution from W-W interactions, and this may in turn account for some of the minor discrepancies amongst the data series in Fig. 10.

5. Conclusions

The diffusion of tungsten in low W-concentration Cr-W alloys was studied both experimentally in finite-source diffusion measurements and computationally with both the activation-relaxation technique (ART) and molecular dynamics (MD). Experimentally, it was determined that the activation energy of diffusion in the Cr-W system was $Q = 386 \pm 33$ kJ/mol. The results from the computational approach gave activation energies of $Q = 315 \pm 20$ kJ/mol calculated from ART and $Q = 310 \pm 18$ kJ/mol calculated from MD, which are about 20% different from the experimental results. However, the agreement of the individual diffusivities is good and within the uncertainty of the models when examined on the basis of the diffusivity values themselves.

The solute diffusion model used in both computational approaches in this work generally requires that the solute concentration is less than 1–2% [15]; however, the experimental method contained concentrations near the interface as high as 7 atomic % tungsten. W-W pairs were found to be drastically favored over lone W atoms in the simulations, supporting the possibility that higher order W clusters could form and alter the overall W diffusion rate in Cr. This could be one contribution to the mild differences seen between the computationally and experimentally determined diffusivities.

Acknowledgements

This study was supported by the US Defense Threat Reduction Agency under Grant No. HDTRA1-11-1-0062 and by the US Army Research Office under Grant No. W911NF-09-1-0422. MP acknowledges support through a Kwan-Jung scholarship. KCA acknowledges support from a DOE Computational Science Graduate Fellowship under Grant No. DE-FG02-97ER25308 and support from the Fannie and

John Hertz Foundation.

References

- [1] J. Askill, D.H. Tomlin, Self-diffusion in chromium, *Philos. Mag.* 11 (1965) 467–474.
- [2] J. Stephens, W. Klopp, High-temperature creep of polycrystalline chromium, *J. Less Common Met.* 27 (1972) 87–94.
- [3] J. Mundy, C. Tse, W. McFall, Isotope effect in chromium self-diffusion, *Phys. Rev. B.* 13 (1976) 2349–2357.
- [4] J. Campbell, C. Schulte, Positron trapping and self-diffusion activation energies in chromium, *Appl. Phys.* 152 (1979) 149–152.
- [5] J.N. Mundy, H.A. Hoff, J. Pelleg, S.J. Rothman, L.J. Nowicki, Self-diffusion in chromium, *Phys. Rev. B.* 24 (1981) 658–665.
- [6] J. Johansson, a. Vehanen, J. Yli-Kaupilla, P. Hautojärvi, P. Moser, Positron lifetime measurements on electron-irradiated chromium, *Radiat. Eff.* 58 (1981) 31–33.
- [7] M.W. Finnis, J.E. Sinclair, A simple empirical N-body potential for transition metals, *Philos. Mag. A.* 50 (1984) 45–55.
- [8] H. Schultz, Defect parameters of bcc metals: group-specific trends, *Mater. Sci. Eng. A.* 141 (1991) 149–167.
- [9] J. Askill, Tracer diffusion in the chromium–nickel system, *Phys. Stat. Sol. (a).* 8 (1971) 587–596.
- [10] A.D. Le Claire, Application of diffusion theory to the body-centered cubic structures, in: *Diffusion in Body-Centered Cubic Metals*, 1964: pp. 3–24.
- [11] W.C. Hagel, Self-diffusion in solid chromium, *Trans. Metall. Soc. AIME.* 224 (1962) 430.
- [12] H.W. Paxton, E.G. Gondolf, Rate of self-diffusion in high purity chromium, *Arch. Fur Eisenhüttenwes.* 30 (1959).
- [13] P.L. Gruzin, S. V. Zemskii, I.B. Rodina, J.J. Cornish, Study of diffusion of carbon and molybdenum in chromium, Atomic Energy Research Establishment, Harwell, Berkshire, England, 1965.
- [14] N. Peterson, Self-diffusion in pure metals, *J. Nucl. Mater.* 69 (1978) 3–37.
- [15] A.D. Le Claire, Solute diffusion in dilute alloys, *J. Nucl. Mater.* 70 (1978) 70–96.
- [16] G. Bonny, R.C. Pasianot, D. Terentyev, L. Malerba, Iron chromium potential to model high-chromium ferritic alloys, *Philos. Mag.* 91 (2011) 1724–1746.

- [17] J. Wallenius, I.A. Abrikosov, R. Chakarova, C. Lagerstedt, L. Malerba, P. Olsson, et al., Development of an EAM potential for simulation of radiation damage in Fe–Cr alloys, *J. Nucl. Mater.* 329-333 (2004) 1175–1179.
- [18] G. Bonny, N. Castin, J. Bullens, A. Bakaev, T.C.P. Klaver, D. Terentyev, On the mobility of vacancy clusters in reduced activation steels: an atomistic study in the Fe-Cr-W model alloy, *J. Phys. Condens. Matter.* 25 (2013) 315401.
- [19] A.J. Mortlocks, D.H. Tomlin, The atomic diffusion of chromium in the titanium-chromium system, *Philos. Mag.* 4 (1959) 628–643.
- [20] O. Fedchenko, S. Protsenko, P. Zukowski, M. Marszalek, Determination of diffusion coefficients in film systems on the basis of Fe/Cr and Cu/Cr, *Vacuum.* 86 (2012) 1934–1938.
- [21] M. Danielewski, J. Dąbek, S. Mrowec, G. Siemińska, Chemical diffusion in nonstoichiometric chromium sulfide, $\text{Cr}_{2+y}\text{S}_3$, *Solid State Ionics.* 17 (1985) 331–335.
- [22] J. Čermák, J. Růžičková, A. Pokorna, Low-temperature tracer diffusion of chromium in Fe-Cr ferritic alloys, *Scr. Mater.* 35 (1996) 411–416.
- [23] F.J.A. Den Broeder, Interface reaction and a special form of grain boundary diffusion in the Cr-W system, *Acta Metall.* 20 (1972) 319–332.
- [24] T. Chookajorn, H.A. Murdoch, C.A. Schuh, Design of Stable Nanocrystalline Alloys, *Science.* 337 (2012) 951–954.
- [25] H.A. Murdoch, C.A. Schuh, Stability of binary nanocrystalline alloys against grain growth and phase separation, *Acta Mater.* 61 (2013) 2121–2132.
- [26] N. Mousseau, G. Barkema, Traveling through potential energy landscapes of disordered materials: The activation-relaxation technique, *Phys. Rev. E.* 57 (1998) 2419–2424.
- [27] N. Mousseau, L.K. Béland, P. Brommer, J.-F. Joly, F. El-Mellouhi, E. Machado-Charry, et al., The Activation-Relaxation Technique: ART Nouveau and Kinetic ART, *J. At. Mol. Opt. Phys.* 2012 (2012) 1–14.
- [28] S. Plimpton, Large-scale atomic/molecular massively parallel simulator, Sandia National Laboratories: [Http://lammps.sandia.gov](http://lammps.sandia.gov). (1995).
- [29] S. Plimpton, Fast Parallel Algorithms for Short-Range Molecular Dynamics, *J. Comput. Phys.* 117 (1995) 1–19.
- [30] C.A. Becker, Atomistic simulations for engineering: Potentials and challenges, Tools, Models, Databases and Simulation Tools Developed and Needed to Realize the Vision of ICME. ASM (2011).
- [31] M. Daw, M. Baskes, Embedded-atom method: Derivation and application to impurities, surfaces, and other defects in metals, *Phys. Rev. B.* 29 (1984) 6443–6453.

- [32] A. Stukowski, B. Sadigh, P. Erhart, A. Caro, Efficient implementation of the concentration-dependent embedded atom method for molecular-dynamics and Monte-Carlo simulations, *Model. Simul. Mater. Sci. Eng.* 17 (2009) 075005.
- [33] C.L. Kelchner, S.J. Plimpton, J.C. Hamilton, Dislocation nucleation and defect structure during surface indentation, *Phys. Rev. B.* 58 (1998) 11085–11088.
- [34] D. Rodney, C.A. Schuh, Yield stress in metallic glasses: The jamming-unjamming transition studied through Monte Carlo simulations based on the activation-relaxation technique, *Phys. Rev. B.* 80 (2009) 184203.
- [35] E. Cancès, F. Legoll, M.-C. Marinica, K. Minoukadeh, F. Willaime, Some improvements of the activation-relaxation technique method for finding transition pathways on potential energy surfaces., *J. Chem. Phys.* 130 (2009) 114711.
- [36] D.S. Watkins, *The Matrix Eigenvalue Problem*, Society for Industrial and Applied Mathematics, Philadelphia, 2007.
- [37] J. Manning, Correlation factors for impurity diffusion. bcc, diamond, and fcc structures, *Phys. Rev.* 819 (1964).
- [38] K.C. Alexander, C.A. Schuh, Exploring grain boundary energy landscapes with the activation-relaxation technique, *Scr. Mater.* 68 (2013) 937–940.
- [39] G.H. Vineyard, Frequency factors and isotope effects in solid state rate processes, *J. Phys. Chem. Solids.* 3 (1957) 121–127.
- [40] E. Anderson, Z. Bai, C. Bischof, S. Blackford, J. Demmel, J. Dongarra, et al., *LAPACK Users' Guide, Third*, Society for Industrial and Applied Mathematics, Philadelphia, PA, 1999.
- [41] H.J.C. Berendsen, J.P.M. Postma, W.F. van Gunsteren, a. DiNola, J.R. Haak, Molecular dynamics with coupling to an external bath, *J. Chem. Phys.* 81 (1984) 3684.
- [42] X. Zhou, H. Wadley, R. Johnson, Atomic scale structure of sputtered metal multilayers, *Acta Mater.* 49 (2001) 4005–4015.
- [43] J. Li, AtomEye: an efficient atomistic configuration viewer, *Model. Simul. Mater. Sci. Eng.* 11 (2003) 173–177.

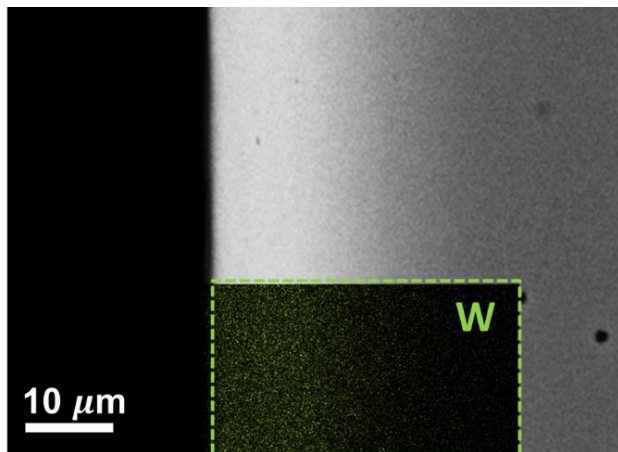


Figure 1. Scanning electron microscopy (SEM) image taken in backscatter mode, for a chromium disc cross section after annealing at 1526 K. A tungsten elemental map from EDS is shown in the inset.

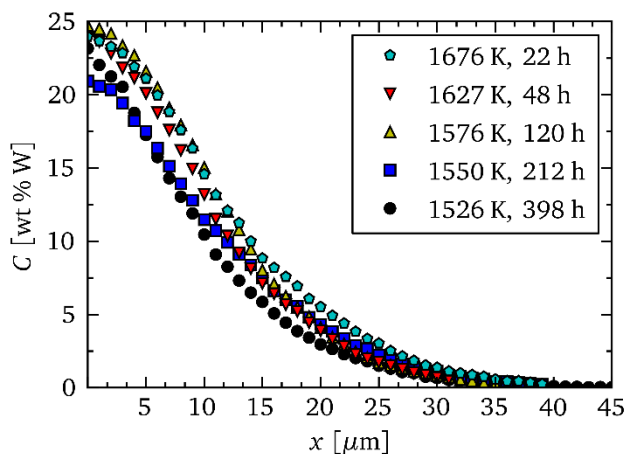


Figure 2. Tungsten concentration versus penetration-distance at five different temperatures from EMPA measurements in a Cr-W diffusion. The diffusion length is zeroed at the initial Cr-W interface.

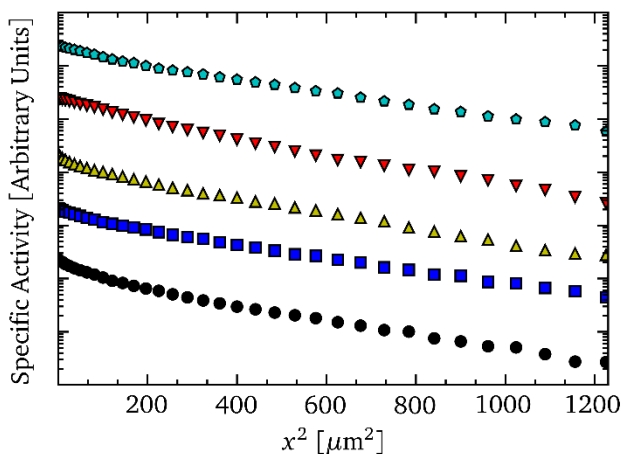


Figure 3. Specific activity versus square-penetration-distance at five different temperatures, presented on a logarithmic scale.

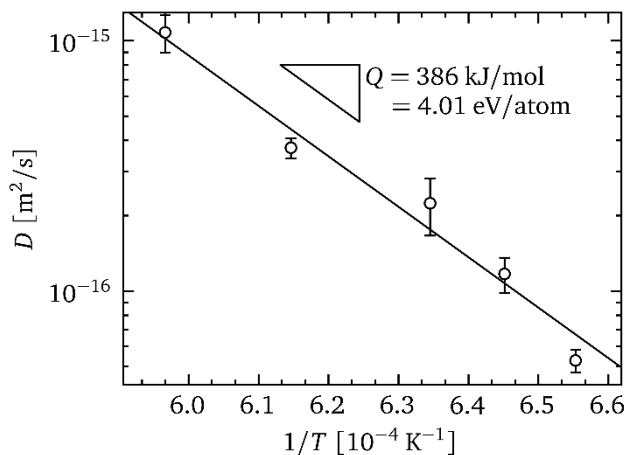


Figure 4. Arrhenius plot of solute diffusion data for Cr-W diffusion experiments. 5–12 depth profiles are represented by each data point, and the error bars correspond to 95% confidence bounds on the mean value of the diffusivity calculated at each temperature.

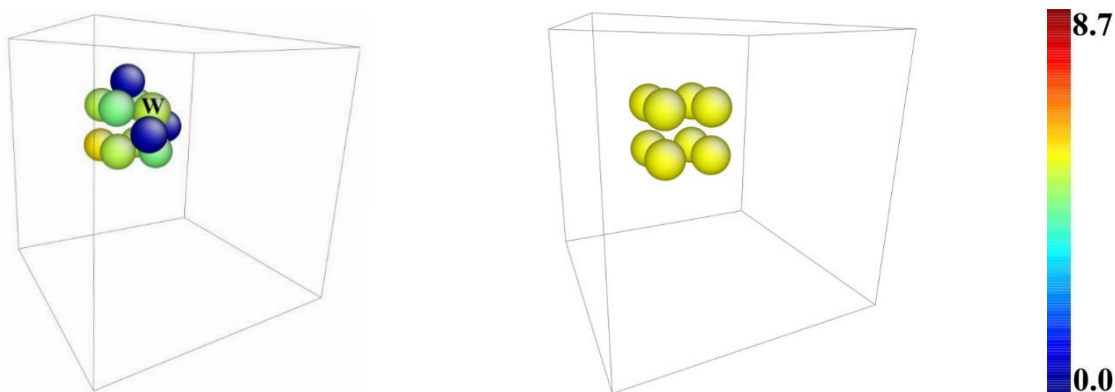


Figure 5. Vacancy structures for the bound and free states found in this study. The image containing W in the vacancy structure (left) is 0.66 eV lower in energy than the free vacancy structure with the W atom in the bulk (right). Atoms with centrosymmetry parameter < 0.5 were excluded from the image for clarity. The images were generated with AtomEye [43].

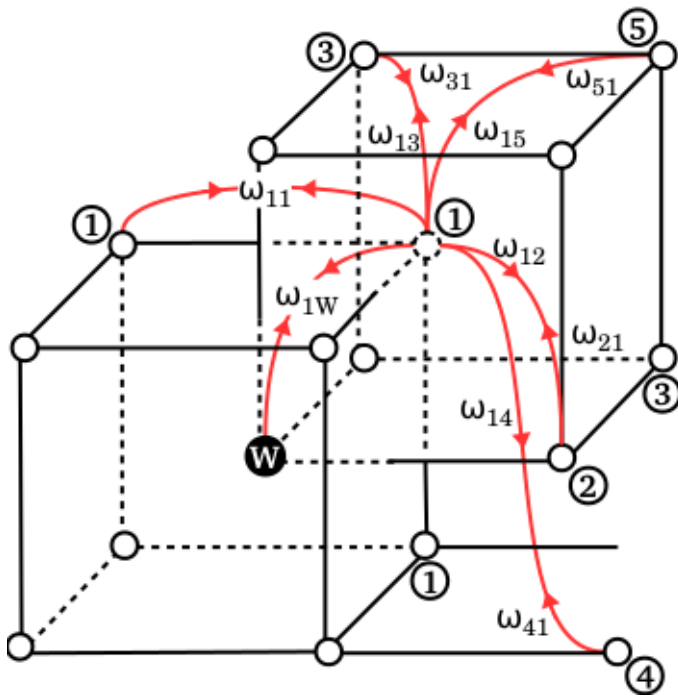


Figure 6. Schematic of the possible jumps relevant to solute diffusion. The vacancy is initially at point 1 and the solute is located in the site marked with the W. Sites of unique vacancy jumps are numbered. Jump frequency from site i to site j is indicated by ω_{ij} and is proportional to the exponential of the activation energy required for the jump. If the forward and reverse activation energies identified by ART were identical for a given transition, then only ω_{1j} is shown in the schematic. This schematic is modeled after Ref. [15].

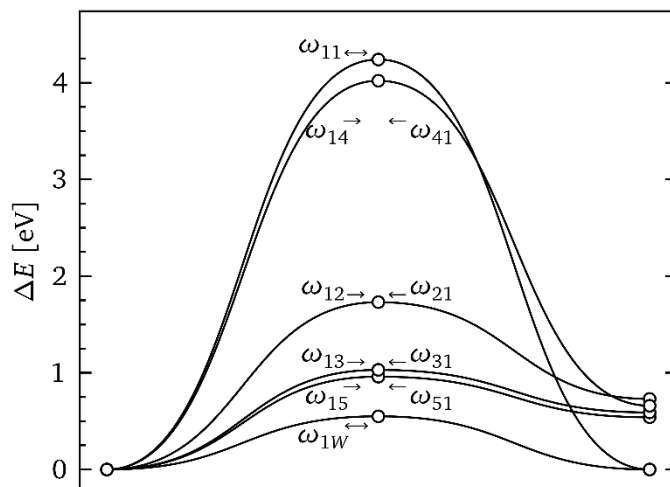


Figure 7. Energy landscape graph of transitions relevant to the diffusion of tungsten in chromium found using ART, plotted on a vertical energy axis. Energy values are plotted relative to the initial minimum energy of the structure. The circles correspond to accessible configurations on the energy landscape and the lines correspond to the pathways connecting them. Forward progress in the transition corresponds to progress along the abscissa. The transitions have been labeled to correspond to the jump frequencies in Figure 6. Only a single label is necessary to denote the symmetric transitions.

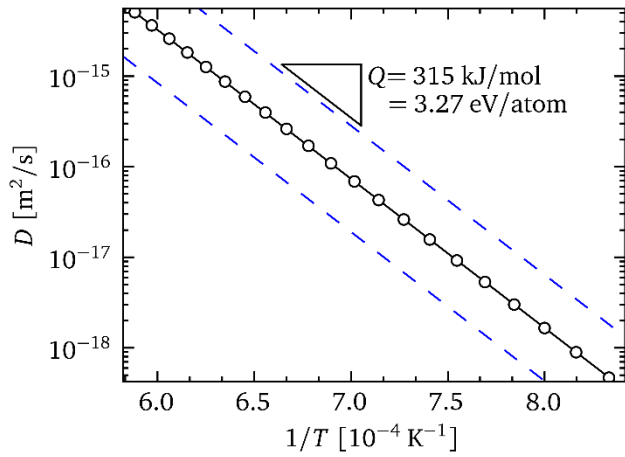


Figure 8. Solute diffusion of W in Cr as generated from Eq. (4), using activation energies determined with ART.

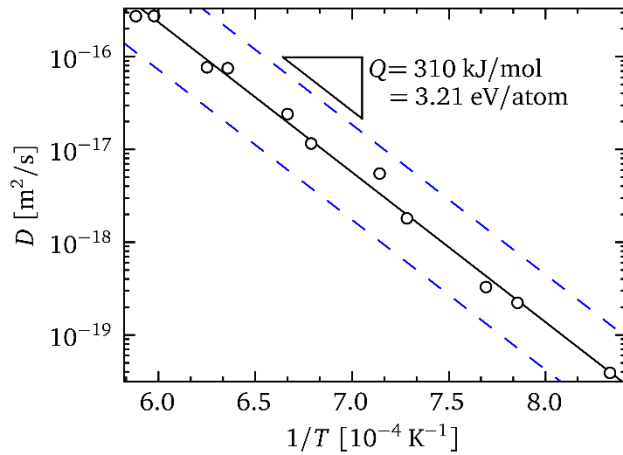


Figure 9. Arrhenius diffusion data for solute diffusion of W in Cr from MD simulations. The dashed lines indicate the 95% confidence bounds for the value of D.

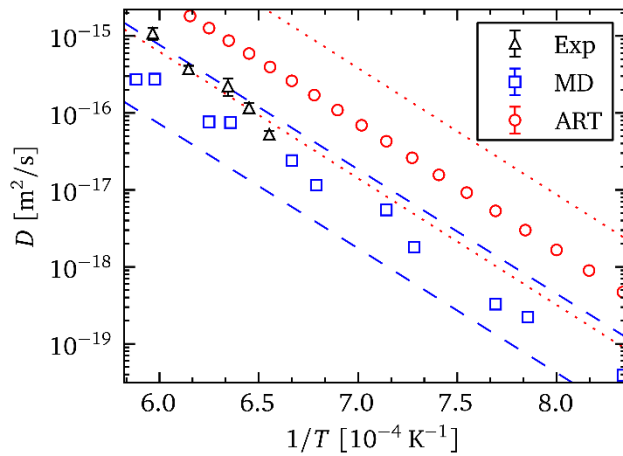


Figure 10. Arrhenius diffusion data for diffusion of W in Cr from experiments, MD simulations, and ART. The blue, dashed lines and black error bars indicate the 95% confidence bounds for the value of D from MD and experiments, respectively.